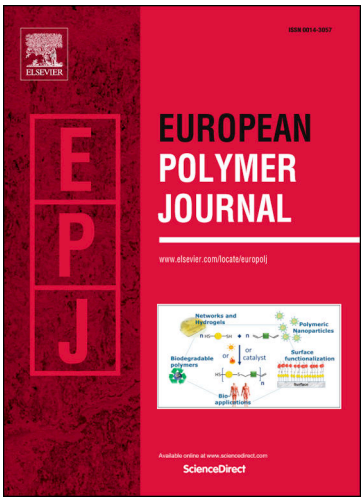

3D printed Artificial Cornea for Corneal Stromal Transplantation

Songul Ulag, Elif Ilhan, Ali Sahin, Betul Karademir Yilmaz, Deepak M. kalaskar, Nazmi Ekren, Osman Kilic, Faik Nuzhet Oktar, Oguzhan Gunduz

PII: S0014-3057(20)30151-8
DOI: https://doi.org/10.1016/j.eurpolymj.2020.109744
Reference: EPJ 109744

To appear in: *European Polymer Journal*

Received Date: 19 January 2020
Revised Date: 2 May 2020
Accepted Date: 4 May 2020

Please cite this article as: Ulag, S., Ilhan, E., Sahin, A., Karademir Yilmaz, B., kalaskar, D.M., Ekren, N., Kilic, O., Nuzhet Oktar, F., Gunduz, O., 3D printed Artificial Cornea for Corneal Stromal Transplantation, *European Polymer Journal* (2020), doi: https://doi.org/10.1016/j.eurpolymj.2020.109744

3D printed Artificial Cornea for Corneal Stromal Transplantation

Songul Ulag[a, b], Elif Ilhan[a, c], Ali Sahin[d, e], Betul Karademir Yilmaz[d, e], Deepak M. kalaskar [f], Nazmi Ekren[a, g], Osman Kilic[a, h], Faik Nuzhet Oktar[a, c], Oguzhan Gunduz[a, i]

[a]Center for Nanotechnology & Biomaterials Application and Research (NBUAM), Marmara University, Turkey
[b]Department of Metallurgical and Materials Engineering, Institute of Pure and Applied Sciences, Marmara University, Turkey
[c]Department of Bioengineering, Faculty of Engineering, Marmara University, Turkey
[d]Department of Biochemistry, Faculty of Medicine, Marmara University, Turkey
[e]Genetic and Metabolic Diseases Research Center (GEMHAM), Marmara University, Turkey
[f]UCL Division of Surgery and Interventional Science, Royal National Orthopaedic Hospital, Brockley Hill, HA7 4LP
[g]Department of Electric and Electronics Engineering, Faculty of Technology, Marmara University, Turkey
[h]Department of Electric and Electronics Engineering, Faculty of Engineering, Marmara University, Turkey
[i]Department of Metallurgical and Materials Engineering, Faculty of Technology, Marmara University, Turkey

ucemogu@ucl.ac.uk

Abstract

The aim of this study is to understand the optical, biocompatible, and mechanical properties of chitosan (CS) and polyvinyl-alcohol (PVA) based corneal stroma constructs using 3D printing process. Corneal stroma is tested for biocompatibility with human adipose tissue-derived mesenchymal stem cells (hASCs). Physico-chemical and chemical characterization of the construct was performed using scanning electron microscopy (SEM), fourier transforms infrared spectroscopy (FTIR). Optical transmittance was analyzed using UV-Spectrophotometer. Results showed fabricated constructs have required shape and size. SEM images showed construct has thickness of 400 μm. The FTIR spectra demonstrated the presence of various predicted peaks. The swelling and degradation studies of 13%(wt)PVA and 13%(wt)PVA/(1, 3, 5)%(wt)CS showed to have high swelling ratios of 7 days and degradation times of 30 days, respectively. The light transmittance values of the fabricated cornea constructs decreased with CS addition slightly. Tensile strength values decreased with increasing CS ratio,

but we found to support intraocular pressure (IOP) which ranges from 12 to 22 mm-Hg. Preliminary biostability studies showed that composite constructs were compatible with hASCs even after 30 days' of degradation, showing potential for these cells to be differentiated to stroma layer in future. This study has implications for the rapid and custom fabrication of various cornea constructs for clinical applications.

Keywords: corneal stroma; chitosan; mesenchymal stem cell; polyvinyl-alcohol; 3D printing.

1.Introduction

The cornea is a protective clear outer layer that is placed at the forefront of the eye. It's shape is oval and it lies in front of the iris, pupil and anterior chamber. The cornea has responsibility for light transmission and reflection to focus on the retina [1, 2]. Corneal blindness can occur due to corneal trauma and ulceration, infections caused by bacteria and environmental conditions. Over ten million individuals have affected this disease in the world and the human body cannot repair the corneal endothelial cells. Therefore, cornea transplant is the only treatment for corneal diseases by replacing diseased corneas with a healthy one for restoring vision [3, 4]. However, cornea transplants are associated with infections, immunological rejection and most importantly availability of adequate donor corneas [4, 5]. Nowadays, many countries included developed countries, face a serious lack of donors. In countries where corneal blindness cases are increasing, the proportion of healthy donor tissue is also very low. Therefore there is an urgent need to find alternative solutions to replace the damaged cornea with an artificial cornea. There are two strategies to develop artificial cornea. One is corneal equivalent which uses biomaterials to reconstruct the cornea [6]. The other one is keratoprostheses (KPros) implantation that contains removal of all damaged cornea and replacing by an artificial cornea. However, some important disadvantages can be observed such as infectious keratitis, prosthetic material melting, device extrusion, etc [7]. Furthermore, the formation of a membrane may cause complications in keratoprosthesis [8]. To solve these

problems, tissue engineering approaches have become an important solution that contains cells, scaffold carriers, and tissues [9]. A huge amount of research has been directed for producing tissue-engineered cornea but there are still a large number of challenges. To get ideal corneal structures, there are some factors to be considered which are transparency, suitable mechanical and chemical properties, oxygen permeability, biodegradability, and biocompatibility [10]. The aim of this study is to construct the tissue-engineered artificial cornea which is able to provide the above features and bring new treatment for corneal blindness by using 3D printing technology which allows mimicking both the structure and the geometry of the human cornea. It is sufficient to fabricate the complex geometries using the 3D printing device compared to the mould casting. 3D printing can allow mimicking the exact shapes of the tissues. With mould casting, it is not easy to adjust the thickness and pore size values of the structures exactly. However, 3D printing is a functional process for building the complex geometries with also mimicking of each layer. It is a novel and better method compared to the other production techniques and it provides to control of pore size, porosity, and complex shapes of the tissue scaffolds [11].

In this study, corneal constructs contain polyvinyl alcohol (PVA) and low molecular weight Chitosan (CS) which are widely used in biomedical applications. PVA is a synthetic hydrophilic polymer, which is biocompatible and biodegradable. Its hydrogel form extensively used in the field of tissue engineering to repair and regenerate the tissues. It has high availability for arterial phantom, heart valves, corneal implants, and cartilage tissues. Furthermore, it should be added that PVA is supportive for the development of oxygen permeability which is an essential property for corneal tissue engineering [12]. There are some studies which use the gelatin [13], alginate [14], collagen [14], and so on as a substrate for corneal tissue. However, PVA has been generally used as carrier in cornea tissue engineering on account of its transparency, elasticity and mechanical stability compared to the natural polymer based scaffolds [15]. Chitosan

polysaccharide is produced from the deacetylation of chitin and it has been used in tissue engineering due to their non-toxicity, biodegradability, high permeability and antibacterial properties. Chitosan is effective to increase a precorneal residence time of antibiotics than other commercial solutions [16]. Chen et al [17] combined the Collagen/Chitosan/Sodium Hyaluronate and showed that this blends are non-cytotoxic by using rabbit corneal cells. In the present study, CS was combined with PVA as a potential artificial cornea scaffold that can provide functional corneal stroma. Thinking about the toxic effect of crosslinkers, PVA and Chitosan were combined without using any conventional chemical crosslinking agents and reagents [18].

2. Materials and method

2.1. Materials

Polyvinyl alcohol (PVA, MW=89000-98000) and low molecular weight Chitosan (CS, MW=50000-190000 Da) were supplied by Sigma Aldrich (USA). Acetic acid glacial (CH_3COOH, M=60.05 g/mol) was purchased from Merck Company (Germany).

2.2. Method

In the first part of the study, corneal support structures that have 12 mm vertical and horizontal diameter values were fabricated by the Orijin Makina company (Istanbul, Turkey). The cornea mold was drawn with the Solidworks program and produced with Aluminum 6063 by using the Machining Strategies program. After the mold fabrication, cornea model was formed with G-code which comes from the transformation of corneal drawing into code via Simplify program. According to this code, cornea structure was printed from bottom to the top layer by layer by using a 3D printing device (Tribot) to get exact cornea shape (Figure 1). Luer-Lock Tip syringe (BD, 10 ml, Belgium) and 25G plastic needle which has nearly 30 mm height value were used during the printing process. Printing parameters were temperature, extrusion multiplier, printing speed, extruder diameter, extruder width, and infill layer interval which were selected as 25°C,

40, 100%, 0.5 mm, 0.6 mm, and 1, respectively. In this study, the printing speed was set as 100% which indicates that it multiplied the default printing speed value (6 mm/s) with the percentage of 100.

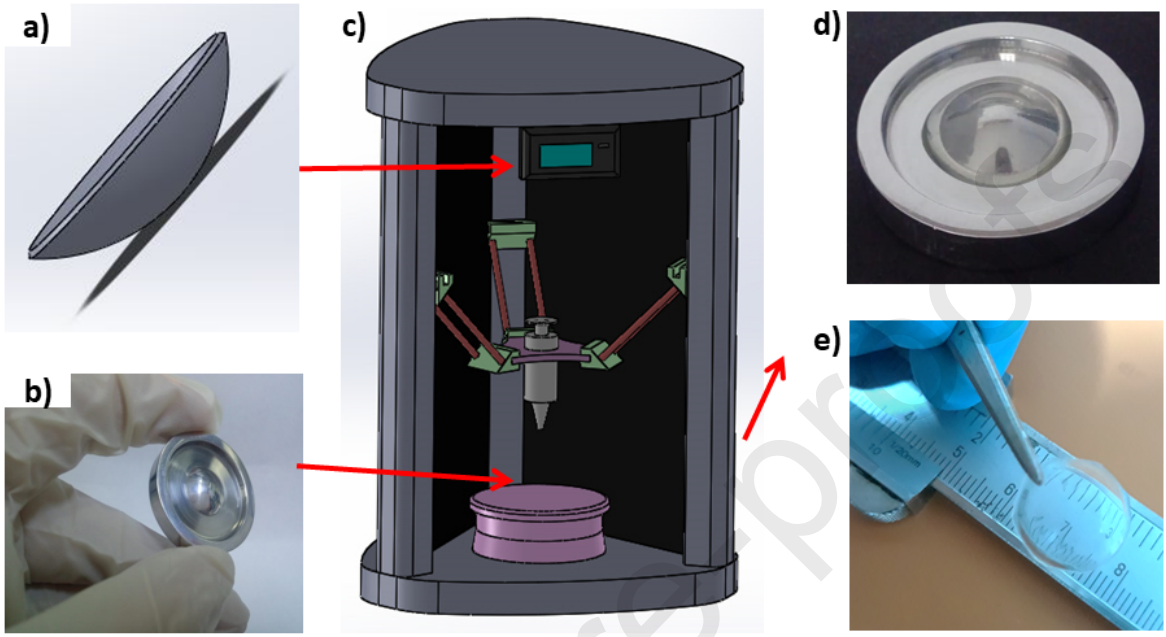

Figure 1. The printing steps for production of corneal construct, solid model (a), Aluminium mold (b), 3D device (c), after printing process (d), printed corneal stroma construct (e).

2.3. Production of the 13%(wt)PVA/(1, 3, 5)%(wt)CS composites

1.3 g PVA was mixed with 10 mL distilled water at 90 °C to obtain a homogenous 13%(wt)PVA solution by shaking for 6 hrs. (1, 3, 5)%(wt)CS particles were dissolved in 2% acetic acid and distilled water solution. Then, these solutions were added into the 13%(wt)PVA solution separately to get 13%(wt)PVA/(1, 3, 5)%(wt)CS solutions and corneal stroma constructs.

2.4. Characterization of the printed structures

2.4.1. FTIR analysis

The chemical characterization of the composites was examined by a fourier transform infrared spectroscopy (FTIR, JASCO-4000). All spectrums were taken at 4000-400 cm^{-1} scanning range with a resolution of 4 cm^{-1} in the absorbance mode.

2.4.2. SEM investigations

Scanning electron microscopy (SEM, ZEISS MA/EVO10) was used to examine the morphological characterization of the composites. They were mounted with Au for the 60s by using Quorum SC7620 coater before analysis.

2.4.3. Differential scanning calorimetry (DSC)

DSC was used for the thermal transition behavior of the printed constructs by using Shimadzu DSC-60 Plus machine which has a 25–600 °C temperature range and calorimetric measuring range: ±150 mW. The constructs were scanned at a constant heating rate of 10°C/min.

2.4.4. Swelling and degradation tests

The swelling and degradation characteristics of the printed constructs were determined with swelling and degradation tests. Printed constructs were submerged in phosphate buffer saline (PBS, pH=7) at 37°C using a thermoshaker (BIOSAN TS-100C) with 250 revolutions per minute. In the swelling test, printed constructs were immersed in PBS for 1, 2, 3, 4, 5, 6, 7 days. The same PBS was used during the swelling test. The swelling rate (S_R) of the composites was calculated according to the equation 2.1:

$$S_R=\frac{W_S-W_D}{W_D}.100 \quad (2.1)$$

W_S and W_D were swollen weight (weight of the composite at each time), and dry weight before the swelling process, respectively.

In the degradation study, constructs were submerged in a PBS for a month and measurements were recorded twice a week. PBS was changed after each measurement during the degradation test. Equation 2.2 was used to calculate the weight loss (W_L), where W_0 refers to the initial weight and W_d is the dried weight [19]. Swelling and degradation values for all constructs were normalized to 100% as an initial value to compare the data with each other easily.

$$W_L=\frac{W_0-W_d}{W_0}.100 \quad (2.2)$$

2.4.5. Uniaxial tensile testing

The tensile test was applied to measure the mechanical resistance of the dry printed corneal stroma constructs against the intraocular pressure. Stress vs strain curve of the composites was determined with a uniaxial tensile test using a Shimadzu tensile device. Constructs were put directly between the jaws. The tensile test also performed using the degrade constructs for each concentration with one sample to observe the mass change effect on mechanical properties.

2.4.6. UV spectrophotometer for optical transmittance

The light transmittance percentage of the composites which has an important parameter for the cornea were tested by T-80 UV/VIS Spectrophotometer (PG Instruments Ltd) in the visible region. To determine the exact transmittance values, experiments were repeated three times and their averages were taken to get the mean transmittance values for all constructs. The test was performed in air for all constructs and before the measurement the baseline was obtained to remove the backgorund in the analysis.

2.4.7. Oxygen permeability measurements

Oxygen permeability measurements were carried out using an extra solution perme O_2 single cell. PermeO_2 is used to measure oxygen permeability with temperature and relative humidity control system. The corneal constructs were glued to a metal surface with a hole in the middle using epoxy glue. 100% oxygen gas was used as test gas and temperature and humidity were adjusted to 23°C and 60% room humidity (RH) from both sides, respectively.

2.4.8. Isolation of hASCs, MTT assay, DAPI staining, and fixation protocol for SEM imaging

Human derived adipose tissue cells were cleaned with phosphate-buffered saline (PBS) two times to eliminate extra blood and connective tissues. Stromal vascular fraction (SVF) was acquired after digestion using 0.075% collagenase type II (Biochrom) and agitation at 37°C for 60 min. Then, they were filtrated and centrifugated. Cell pellet was obtained after supernatant was removed and then cell pellet was resuspended in DMEM (Invitrogen), supplemented with

10% fetal bovine serum (FBS, Invitrogen), 1% antibiotic/antimycotic (Invitrogen). DMEM was changed 48 h after initial process and repeated every three days. After isolation at 90% confluence, cells were obtained by plastic adherence and collected after isolation.

3D-printed both non-degradable and degraded corneal stroma constructs were sterilized overnight by Ultraviolet (UV) in 24 well plates. DMEM supplemented with 10% FBS and 0.1 mg/ml penicillin/streptomycin and all constructs were incubated in this medium for an hour at 37° C, 5%CO_2 atmospheres. After an hour, structures were collected and a remaining medium was discarded with a micropipette. Standard cell seeding procedure was made on 3D-printed corneal stroma structures with $4x10^4$ hASCs. The control group (hASCs, $4x10^4$ cells, 200 µl) also incubated at the same time to compare the results. Cells were incubated with 3D corneal structures at 37°C, 5%CO_2 for 1, 3, 7 days. Cytotoxicity detection kit (MTT from Glentham Life Sciences) was used to examine the cytotoxic properties of the corneal structures. Absorbance values were examined at 560 nm wavelength in ELISA reader (Perkin Elmer, Enspire). All measurements were performed in triplicates with 5 samples for all constructs and their averages were performed as the final result.

DAPI staining was done to observe the attachment of MSCs on the 3D-printed structures. The growth medium was removed from the plates and corneal stroma structures were washed with PBS. After that, all stroma constructs were fixed with 4% formaldehyde for 30 min at room temperature and they were washed with PBS. In the next step, 1 µg/ml DAPI (Invitrogen) was added on each stroma constructs to stain the nucleus of the cells and incubated for 20 min at room temperature. Finally, DAPI solution was removed and constructs were taken for imaging under fluorescence inverted microscope (Leica). Standard deviations were used to determine the error bars.

SEM was used to observe the cellular morphology of hASCs on the 3D-printed scaffolds. In the fixation procedure, the growth medium was discarded and all constructs were fixed with

4% glutaraldehyde (Sigma Aldrich). Then, they were dehydrated with diluted ethanol and dried in air. Dried constructs were sputter-coated with Au and examined by using SEM with 10 kV.

3. Results and discussions

3.1. FTIR spectroscopy

Confirmation of the interaction mechanisms between the components was the objective of performing FTIR spectroscopy. Figure 2 showed the FTIR absorbance spectra of the neat polymers and printed constructs. In Figure 2a, there were observed several main peaks at ~3279 cm^{-1}(O-H group, N-H amino group), ~2905.2 cm^{-1}(C-H stretch vibration), ~1417.4 cm^{-1}(C-O), ~1323.9 cm^{-1}(C-H bending), ~1237.1 cm^{-1}(C=O vibration), ~1140.7 cm^{-1}(C-O stretching), ~1086.7 cm^{-1}(C-O group), ~918 cm^{-1}(C-C stretching), ~832.1 cm^{-1}(C-O stretching) for pure PVA [4]. In Figure 2b, the band at ~3283.2 cm^{-1} attributed the stretching groups of –OH and –NH. Symmetric C-H vibration has occurred at ~2869 cm^{-1}. The bands at ~1649 cm^{-1}, ~1589.1 cm^{-1}, ~1374 cm^{-1}, ~1314.3 cm^{-1}, ~1149.4 cm^{-1} and ~1023.1 cm^{-1}, ~893.8 cm^{-1} presented the υ(-C=O) secondary amide, υ(-C=O) protonated amine, δ(C-H), υ_S(-CH_3) tertiary amide, υ_{as} (-C-O-C) and υ_s (C-O-C), ω(C-H), respectively [3]. The peaks at 1071 cm^{-1}-835$cm^{-1}$are due to the representative peaks of the crystallization of chitosan [5]. There were observed some differences between the absorption peaks of the neat PVA and 13%(wt)PVA (Figure 2c): the peak at ~3279.4 cm^{-1} was shifted to ~3253.3 cm^{-1} from pure PVA to 13%(wt)PVA, another absorption band peak for pure PVA was shifted from the ~2905 cm^{-1} to ~2908 cm^{-1} for 13%(wt)PVA. The third absorption band shift was observed at ~1417 cm^{-1} which was shifted to ~1414.5 cm^{-1}. The peaks at ~1237 cm^{-1} and ~1140.7 cm^{-1} for pure PVA were not observed at the absorption band of the 13%(wt)PVA. FTIR spectrums of the CS addition samples were shown in Figure 2 (d, e, f). There were again obtained some shifts in absorption peaks by the addition of CS. The peaks at ~1638.2 cm^{-1} and 1637.3 cm^{-1} were seen for 13%(wt)PVA/3%(wt)CS and 13%(wt)PVA/5%(wt)CS corneal structures, respectively. These

peaks were absorption peaks of CS and this peak was not observed for 13%(wt)PVA/1%(wt)CS. This might be due to the low amount of CS into 13%(wt)PVA.

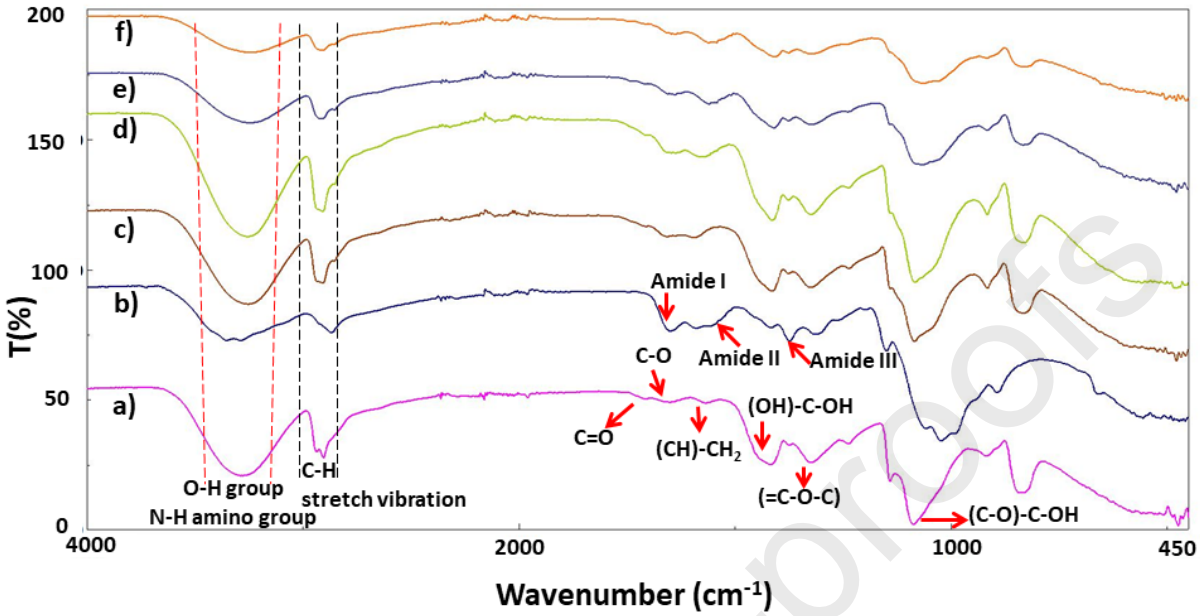

Figure 2. FTIR spectrum of the neat polymers and printed constructs: pure PVA (a), pure CS (b), 13%(wt)PVA (c), 13%(wt)PVA/1%(wt)CS (d), 13%(wt)PVA/3%(wt)CS (e), 13%(wt)PVA/5%(wt)CS (f).

3.2. Morphologic examinations of the printed constructs

The surface and cross-section of 13%(wt)PVA/(1, 3, 5)%(wt)CS blends were examined by SEM to observe the microstructure morphologies of constructs and confirm the compatibility between PVA and Chitosan molecules [20]. In Figure 3 (a, b), the native cornea shape structure of 13%(wt)PVA was seen with 29X magnification and a smooth surface was obtained from the top view of the structure with 500X magnification (Figure 3b). This smooth and homogeneous morphology indicated high homogeneity between PVA and Chitosan. The Hemi-meridional cross-section view of the 13%(wt)PVA/1%(wt)CS was seen in Figure 3c, 3e, and 3f. The mean thickness values of the corneal stroma were calculated using annular averaging at 9 points individually using the cross-sectional view of the stroma. In this study, it was found 136 µm thickness towards the periphery and 400 µm at the center. Stroma thickness is an important parameter for identifying corneal disorders. For instance, it is important to know stromal

thickness values for the early diagnosing of keratoconus. Native stroma forms 90% of the total corneal thickness and it has a central thickness of nearly 478 to 500 µm [21]. Therefore, the thickness value of central stroma found in this study has an acceptable value (400 µm).

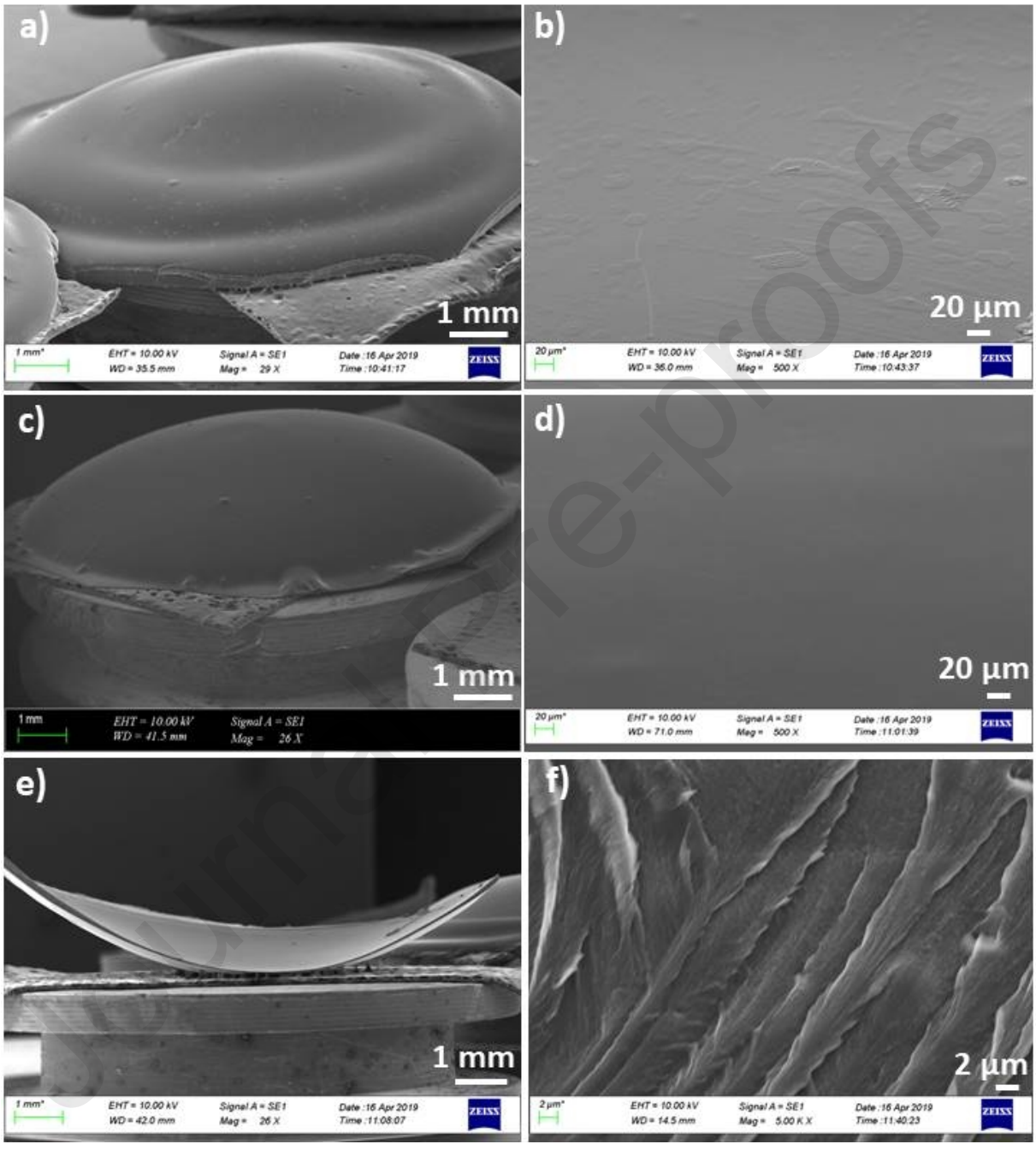

Figure 3. SEM photographs of the 13%(wt)PVA (wt) (a), 13%(wt)PVA/1%(wt)CS (c), cross sectional view of the 13%(wt)PVA/1%(wt)CS (e) and their surface images with high magnifications (b, d), respectively, lamellar structure of the 13%(wt)PVA/1%(wt)CS (f).

3.3. DSC analysis

Figure 4 showed the DSC thermograms of neat PVA, CS, and 13%(wt)PVA, 13%(wt)PVA/(1, 3, 5)%(wt)CS blends. The melting temperature of the 13%(wt)PVA observed at 228.10°C. There was not observed glass transition temperature for 13%(wt)PVA. The degree of crystalline phase and water content in PVA depends on the melting point value. The melting point value for highly crystalline PVA is approximate 230°C [22]. In this study, the melting point was found close to the 230°C and means that 13%(wt)PVA was highly crystalline. However, there was observed that the melting temperature of the 13%(wt)PVA was different when 13%(wt)PVA had in it (1, 3, 5)%(wt)CS. Therefore, the crystalline property of the 13%(wt)PVA was decreased with CS addition. The melting temperatures were 219.47°C, 219.20°C, 216.16°C for 13%(wt)PVA/1%(wt)CS, 13%(wt)PVA/3%(wt)CS, 13%(wt)PVA/5%(wt)CS, respectively. On the other hand, the presence of PVA on the PVA/CS blends could still crystallize and decreasing the melting points could not cause the loss of the melting temperature of PVA [2].

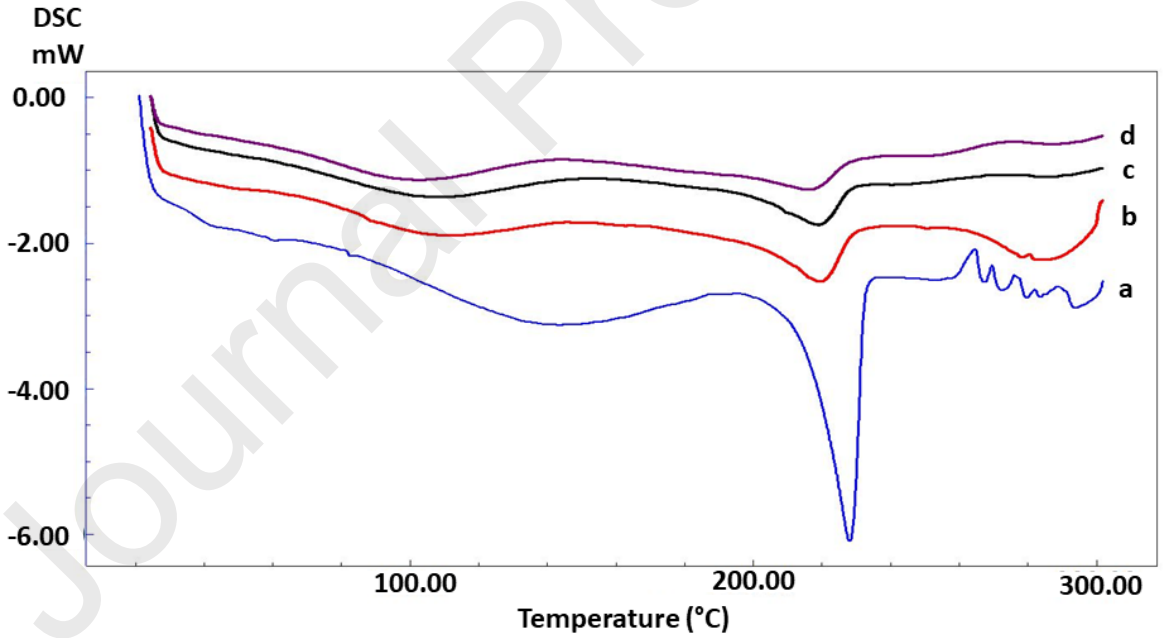

Figure 4. The DSC thermograms of PVA, PVA/CS blends: 13%(wt)PVA (a), 13%(wt)PVA/1%(wt)CS (b), 13%(wt)PVA/3%(wt)CS (c), 13%(wt)PVA/5%(wt)CS (d).

3.4. Swelling and degradation investigations of the corneal structures

3.4.1. Swelling studies

Swelling ability is an important characteristic of a gel. To attain an equilibrium state, gels absorb or release their solvent as a reaction to stimuli of various kinds. Interactions between the polymer network and the solvent affect the equilibrium swelling of gel and these interactions are affected by some external parameters including pH [23]. In this study, pH:7.4 value was used to observe the interactions and absorption ability of gels. It can be deduced from the swelling graph (Figure 5a) that in the initial stage, all constructs absorbed the PBS rapidly and swelling ratio continued at a constant rate over time. The saline absorption of all CS added constructs was more rapidly than 13%(wt)PVA. It might be explained that Chitosan added composite had a more porous structure this provides to transit the water molecules easily between the matrix and added materials [23]. In the present study, swelling capacity was tested in PBS (pH=7.4) at various time points. As shown in Figure 5a, the swelling ability of composites was increased with CS addition compared to the 13%(wt)PVA. It could be said that swelling rates increased with the amounts of chitosan in the solutions [24]. Maximum swelling capacity has been observed for 13%(wt)PVA/5%(wt)CS keeping other factors constant. Since the 13%(wt)PVA/5%(wt)CS displayed maximum swelling, that means that 13%(wt)PVA/5%(wt)CS have a high surface area/volume ratio. This property enables cells to attach and grow efficiently in three-dimensional scaffolds [12]. The swelling rate of the 13%(wt)PVA was decreased between the 1st and 7th days nearly 1.6%. This rate was decreased for 13%(wt)PVA/5%(wt)CS from 4.61 (1st day) to 4.01 (7th day) which gave a 13% difference. It is known that high swelling rate decreases the transparency of the cornea [25]. Thus, high swelling values obtained in this study should be decreased with the crosslinking agents to prevent the loss of transparency by minimizing the swelling rate [26]. Seyed et al. crosslinked the PVA/CS blends using 1-Ethyl-3-(3-dimethylamino propyl)-carbodiimide (EDC) and N-Hydroxysuccinimide (NHS) agents in their study to fabricate cornea tissue carrier for cell delivery. The water absorbency of crosslinked PVA/CS was found to be 361% in swelling test

and optical transmittance was found to be 88% in optical clarity test. On the other hand, the rate of swelling does not only depend on crosslinking agents, there are some parameters that should be thinking together which are the weigth ratio of the components, pH, and temperature, etc [27].

3.4.2. *In vitro* degradation studies

Since the kinetics of degradation could affect cell growth, tissue regeneration, and host response, it has significant value in tissue engineering applications [28]. Degradation behavior of 13%(wt)PVA/(1, 3, 5)%(wt)CS blends was examined for an extended time period of four weeks in this presented study. In Figure 5b, it was observed that degradation rates decreased for all corneal structures means that at the initial stage, degrade structures absorb the water highly and then got lower after the 3 days incubation. By adding Chitosan into the PVA, it was seen that the degradation rate increased gradually. 13%(wt)PVA/5%(wt)CS had a higher degradation rate compared to the others during the degradation period. The degradation rate of the 13%(wt)PVA/5%(wt)CS increased from 100% to 152% on the third day. However, 13%(wt)PVA had the lowest degradation rate changed from 100% to 106% which gave 6% difference after 3 days. It can be easily said that degradation property of the 13%(wt)PVA (wt) enhanced proportionally with CS addition. These results could enable researches to reference the degradation behavior of polymeric scaffolds for *in vivo* tissue engineering applications [12].

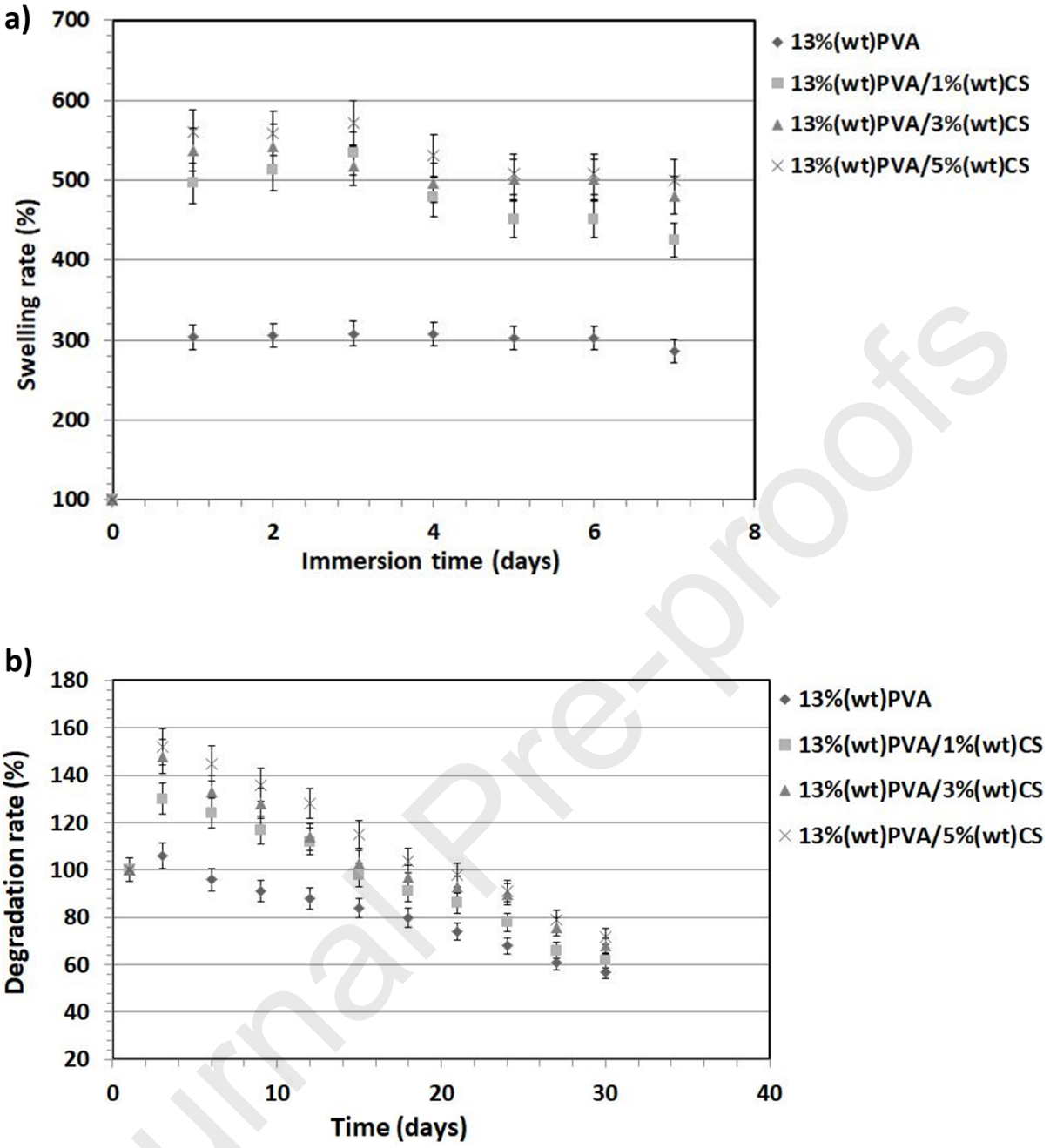

Figure 5. Swelling (a) and degradation (b) profiles of the corneal constructs in phosphate-buffered saline.

3.5. Tensile testing

The examinations of the mechanical behaviors of the corneal structures under forces are of predominant importance. There are many parameters that should be considered to determine the mechanical properties of the composites which are properties of the polymer matrix, the distribution of the fillers, and the features of the interfacial adhesion between the constituents

in the composite [29]. In this study, the mechanical strength of the 13%(wt)PVA and 13%(wt)PVA/(1, 3, 5)%(wt)CS corneal structures were determined by tensile testing which provides the facility of a material to resist breaking under stress. Tensile behavior of the 13%(wt)PVA and 13%(wt)PVA/(1, 3, 5)%(wt)CS composites were included in Figure 6a and Table 1. It was determined that tensile strength values of the 13%(wt)PVA matrix displayed a higher strength value (40.28 MPa) than the 13%(wt)PVA mixture with different amounts of chitosan and minimum tensile strength was seen in 13%(wt)PVA/5%(wt)CS composite. Maximum elongation observed for 13%(wt)PVA/1%(wt)CS. Although 13%(wt)PVA/3%(wt)CS had higher tensile strength, it also had the lowest strain values in all. It can be said that the addition of chitosan particles did not improve the mechanical properties of the final composites. Since the PVA matrix has excellent mechanical properties in itself, the addition of CS into the matrix could not develop the mechanical properties of the final composites [30]. However, the strength values of all constructs still have acceptable values and higher than tensile strength value (3-5 MPa) which is required for corneal tissue engineering [31]. After 30 days of degradation period, tensile test also performed and stress/ strain values and curve of degrading constructs were given in Table 2 and Figure 6b. It was observed significant tensile strength and strain difference between nondegradable and degrade constructs. It was also calculated that the tensile strength difference was 39.76 MPa for 13%(wt)PVA constructs. The elongation at break also decreased from 144.29 to 94.77 MPa after degradation for 13%(wt)PVA construct. The elongation at break values for 13%(wt)PVA/3%(wt)CS and 13%(wt)PVA/5%(wt)CS constructs increased after degradation but their strength values also decreased according to the first situation. After degradation, sharply decreased of tensile strength and elongation at break values could be due to the mass loss of the constructs, which cause the weakening of the constructs. However, these results indicated that constructs after 30 days of degradation period still have strength values even if they are low.

Table 1. Tensile strength and elongation at break values for PVA blended with different concentrations of CS.

Corneal Constructs	Tensile Stress (MPa)	Elongation at break (%)
13%(wt)PVA	40.28	144.29
13%(wt)PVA/1%(wt)CS	11.65	164.01
13%(wt)PVA/3%(wt)CS	12.72	127.16
13%(wt)PVA/5%(wt)CS	8.94	143.19

Table 2. Tensile strength and elongation at break values after 30 days' degradation.

Corneal Constructs	Tensile Stress (MPa)	Elongation at break (%)
13%(wt)PVA	0.52	94.77
13%(wt)PVA/1%(wt)CS	0.51	23.12
13%(wt)PVA/3%(wt)CS	0.35	306.32
13%(wt)PVA/5%(wt)CS	0.72	220.45

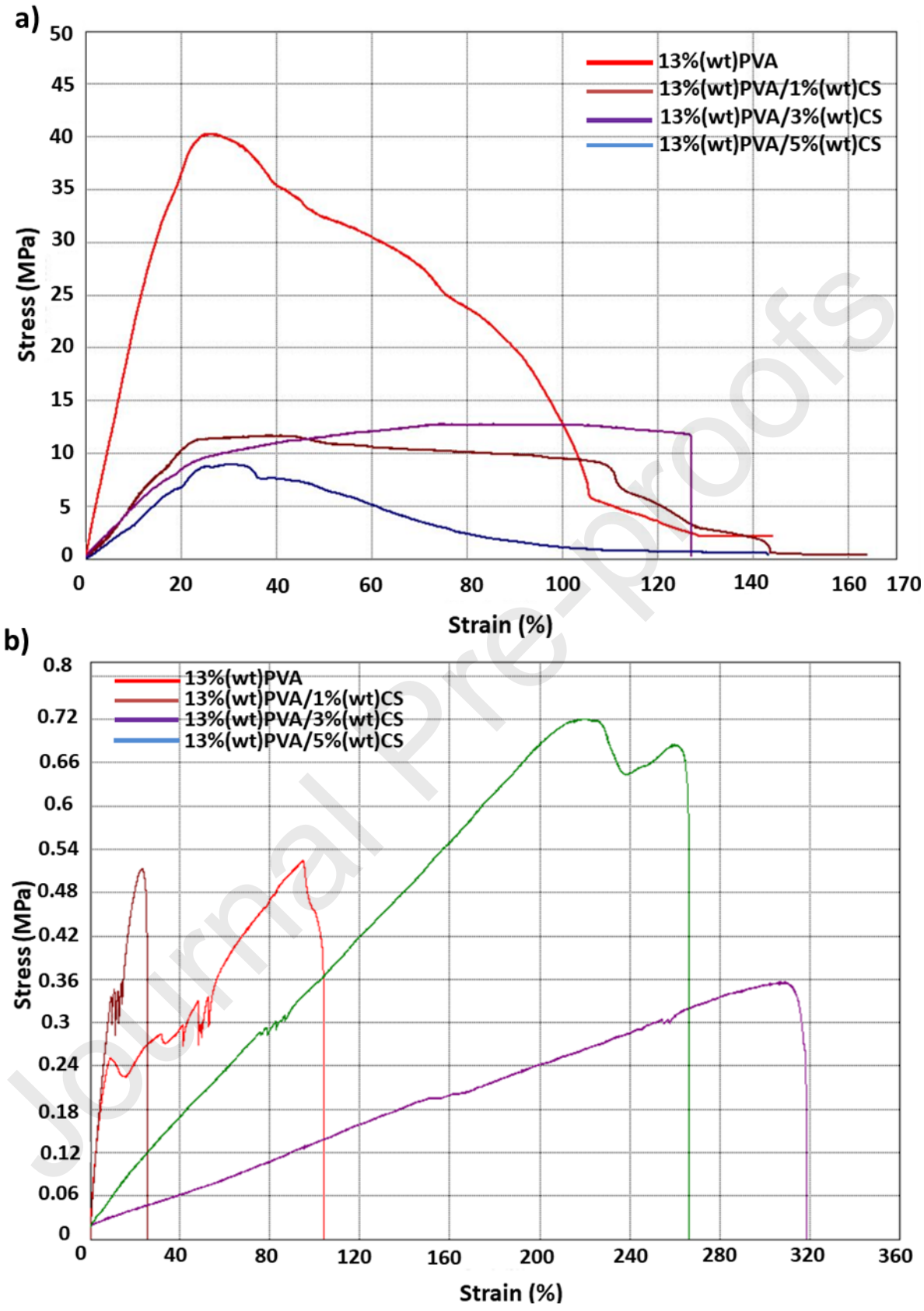

Figure 6. Stress-strain curve in tensile tests of 13%(wt)PVA/(1, 3, 5)%(wt)CS blends: before (a), and after (b) degradation (30 days' incubation).

3.6. Transmittance properties testing

Since the transparent structures provide to examine cell behavior and possible infections, the optical transmittance of printed corneal constructs is important for proper vision [32]. Figure 7 showed the variation in the optical transmission percentage for four different corneal structures as a function of wavelength in the range of 400-800 nm. In order to get rid of the effects of the stroma thickness on the transmittance, it was selected with a thickness of 0.4 mm which value is close to the native cornea thickness [33]. According to the results, it was determined that the corneal stroma constructs had nearly the same transmittance behavior. 13%(wt)PVA had approximately 61% transmission ratio, but with the Chitosan addition, this value decreased to 56%, 53%, and 49% for 13%(wt)PVA/1%(wt)CS, 13%(wt)PVA/3%(wt)CS, 13%(wt)PVA/5%(wt)CS, respectively. At wavelengths shorter than 450 nm, the sharp decreased of 10% was seen in the transmittance values for all corneal stroma constructs. The human cornea has 90% transmittance value [34]. The results obtained from printed constructs showed that the constructs had moderate transmittance value when compared with the human cornea. Therefore, further studies are required to obtain acceptable transmittance value (>90).

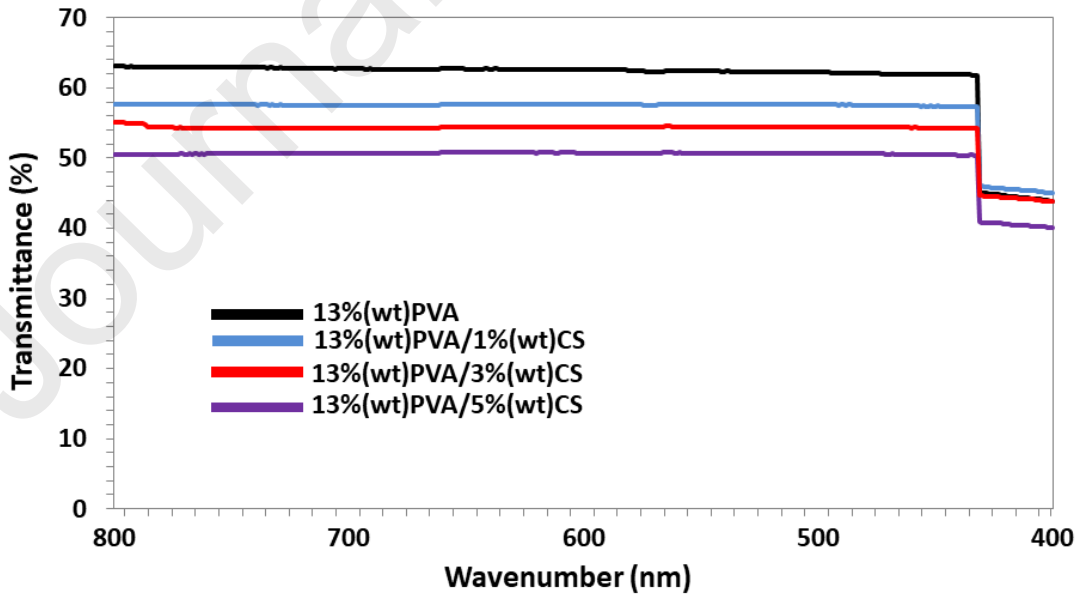

Figure 7. Transmittance through the corneal stroma as a function of wavelength.

3.7. Oxygen permeability results of the stroma constructs

From the point of view of the physiology of the eye, oxygen permeability which provides transport oxygen is an essential parameter to evaluate the availability of corneal structures. The permeability of 100% O_2 through corneal constructs was studied in this presented study. It defines as "D_k" for both cornea and gas permeable plastics. D refers to the oxygen diffusion coefficient and k is the solubility coefficient of a material [35]. The oxygen permeability rates (OTR) were found <0.002, <0.002, <0.002, <0.002, cubic centimeters (cc)/24, for 13%(wt)PVA, 13%(wt)PVA/1%(wt)CS, 13%(wt)PVA/3%(wt)CS, 13%(wt)PVA/5%(wt)CS, respectively (Table 2). According to the results, there were found the same trend between the oxygen permeability values of corneal structures.

Table 2. Oxygen permeability values of the transparent corneal constructs.

Corneal Structures	**D_k (cc/24)**
13%(wt)**PVA**	<0.002
13%(wt)**PVA/1%**(wt)**CS**	<0.002
13%(wt)**PVA/3%**(wt)**CS**	<0.002
13%(wt)**PVA/5%**(wt)**CS**	<0.002

3.8. Cell viability results and cell distribution on corneal stroma constructs

Cellular interaction between cells and artificial tissue construct is a crucial step to test biocompatibility. Therefore, it is essential to produce a non-toxic biocompatible construct that allows cells to bind, adhere and proliferate easily [36]. MTT test was performed to investigate

these cytotoxicity characteristics of the corneal stroma constructs. MTT tests have shown that structures do not negatively affect cell viability and that the interaction between cells and construct is promising, as shown in Figure 8a. MTT assay was performed for 1, 3, and 7 days incubation to determine the hASCs viability of stroma constructs. After 1 day of incubation, cell viability was siginificantly high in the construct containing pure PVA with 158.9%. When the graphs of chitosan containing constructs were analyzed, it was observed that cell viability values for 13%(wt)PVA/1%(wt)CS, 13%(wt)PVA/3%(wt)CS, and 13%(wt)PVA/5%(wt)CS were 91.5%, 118%, and 120.6% respectively. When these results were evaluated, the viability value of pure PVA after initial day incubation was higher than 13%(wt)PVA/(1, 3, 5)%(wt)CS constructs, however, chitosan containing structures still demonstrated good biocompatibility. Although the diminishing in cell viability was observed in all structures after 3 days of incubation, it was analyzed that the cell viability values increased again after 7 days of incubation. After the last day incubation, the cell proliferation values of 13%(wt)PVA, 13%(wt)PVA/1%(wt)CS, 13%(wt)PVA/3%(wt)CS, and 13%(wt)PVA/5%(wt)CS constructs were found to be 75.3%, 89.4%, 79.8%, 90.7%, respectively. The MTT results proved that the fabricated 3D printed corneal stroma constructs are non-toxic, biocompatible, and the cells adapt and proliferate on the formed structure. Baghaie et al. (2017) showed that the cell viability of the constructs that are higher than 75% is considered to be non-toxic according to GB/T 16886.5-2003 (ISO 10993-5: 1999) standards [37]. Peng et al. (2019) reported that the cell viability and proliferation of the Chitosan samples increased gradually compared to pure PVA [38]. As shown, the results of *in vitro* viability tests were compatible with the literature. MTT assay was also performed for 1, 3, and 7 days incubation period to observe the mass change effect on the viability of the hASCs on the degrade 3D-printed corneal stroma constructs. In Figure 8b, when compared to the result with non-degradable constructs, there was a significant decrease in cell viability values of the degraded constructs after 1 day incubation. The viability

values of the 13%(wt)PVA, 13%(wt)PVA/1%(wt)CS, 13%(wt)PVA/3%(wt)CS, 13%(wt)PVA/5%(wt)CS were 38, 49, 36, and 46, respectively. The cell viability value of the 13%(wt)PVA construct was 158.9% before the degradation and the cell viability difference between the non-degradable and degraded constructs was 120 after 1 day culture. On the third day, there was a significant increase in cell viability values for all constructs. The highest rate of increase (111%) was seen for 13%(wt)PVA/1%(wt)CS construct and it was more than control (2D cell line). It can be deduced from these results that even if the mass of the constructs decreases over time, the cells can still enhance and increase their viability values. On the seventh day, cell viability values decreased again, but still much higher than the results obtained on the first day. When the viability values of the degraded and non-degradable constructs were compared, the increase was observed in the viability values of the cultured cells, especially for the 3rd day. The reason for this can be explained as all constructs had a good degradation behavior and this could enhance the survival of the cells [39].

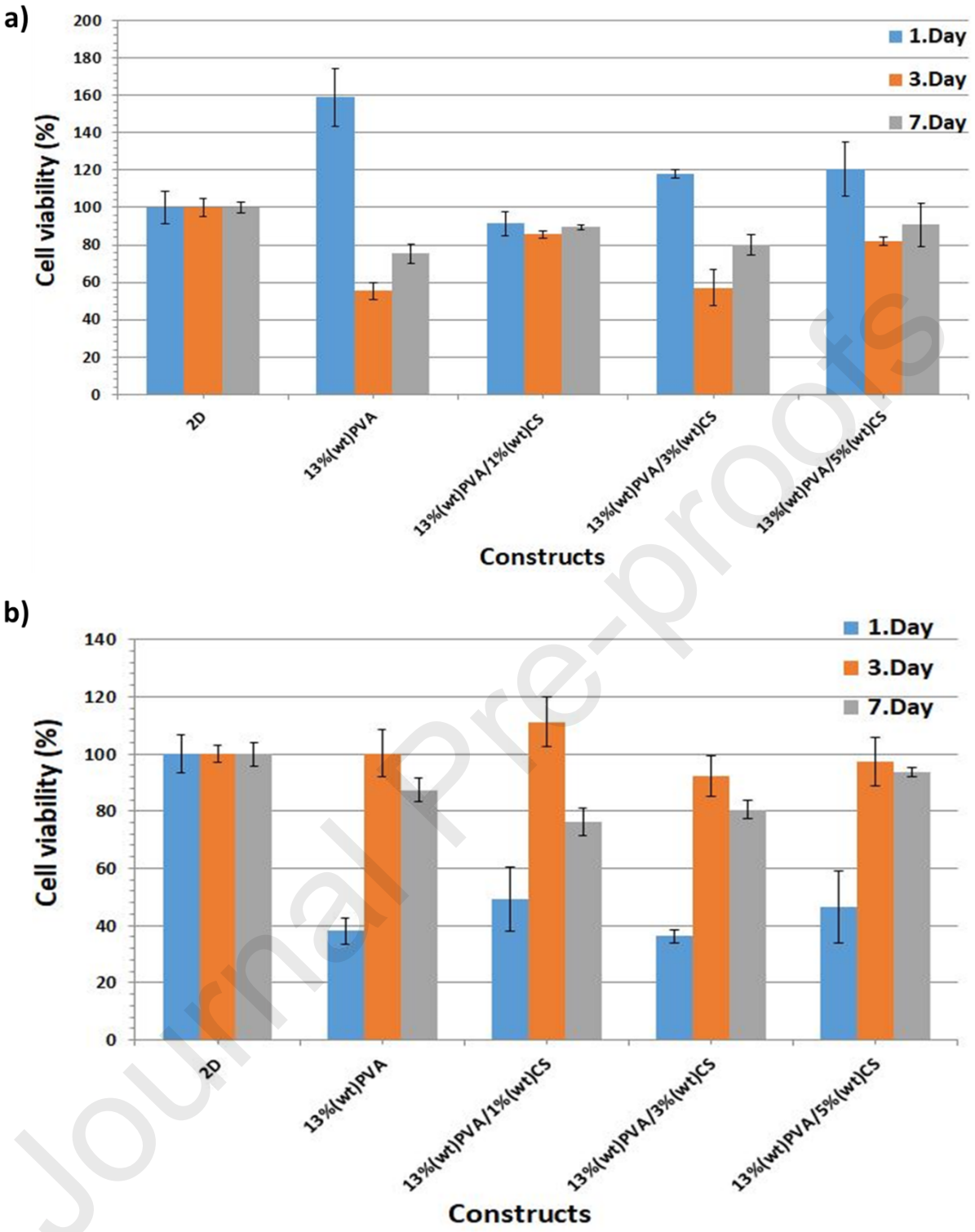

Figure 8. MTT assay results of 2D hASCs and all non-degradable (a) and degraded (b) corneal stroma constructs after 1, 3, and 7 days incubation.

In Figure 9, it was seen that the number of the cells and their shapes were nearly identical. All constructs showed a typical round shape. However, the cell density of the

13%(wt)PVA/1%(wt)CS construct was less when compared to the others for 1-day incubation. Its cells on the surface showed the spheroid-like colonies [40]. After 3 days of culture, a small decrease in the number of cells was observed for 13%(wt)PVA, 13%(wt)PVA/3%(wt)CS, and 13%(wt)PVA/5%(wt)CS. On the other hand, an increase in the number of cells of the 13%(wt)PVA/1%(wt)CS construct was observed compared to the first day. When the 7-day culture results were examined, in general, the number of cells for all structures decreased compared to days 1 and 3. Only the number of cells on the surface of the 13%(wt)PVA/3%(wt)CS construct was higher than on day 3.

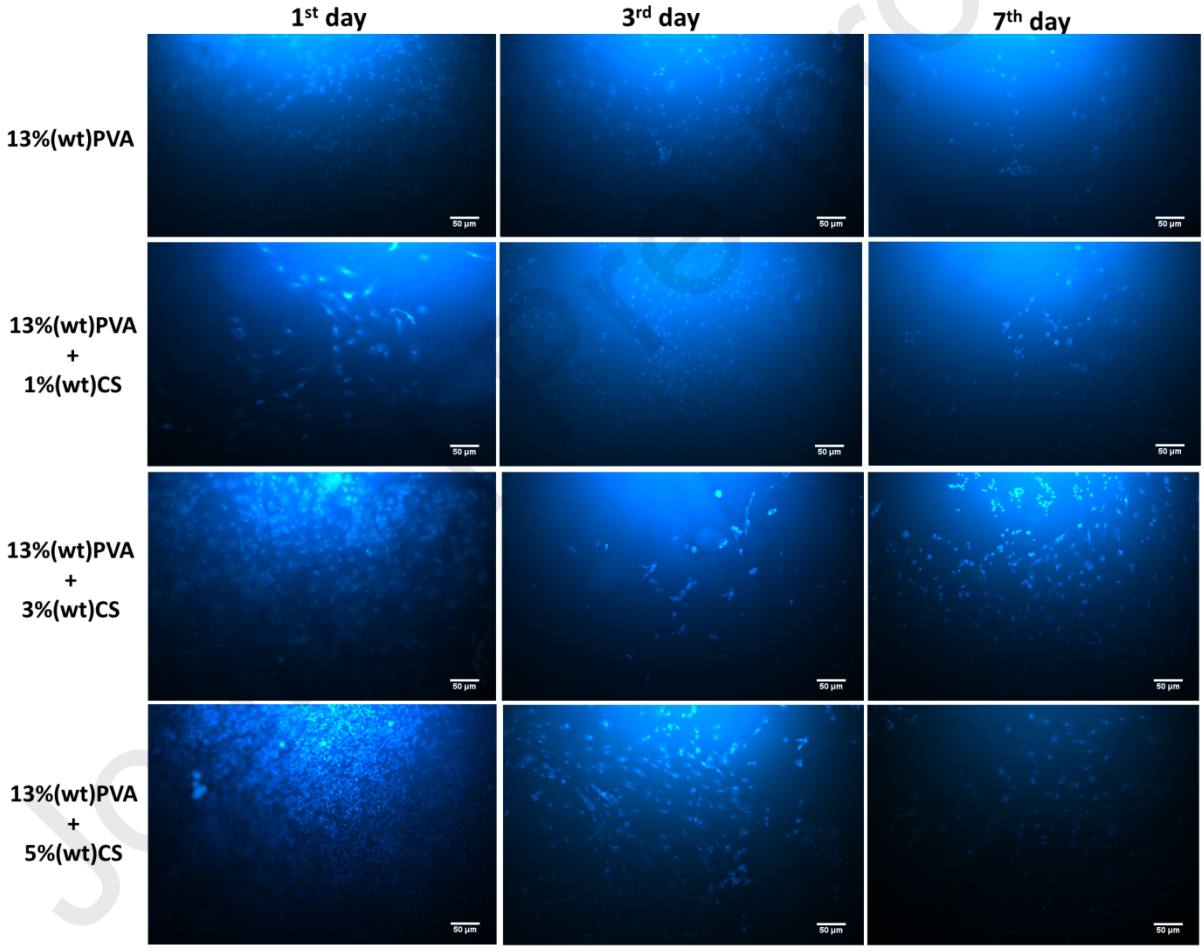

Figure 9. Fluorescence microscopy representation of the corneal stroma constructs with live cells. Nuclei were with DAPI.

3.9. Distribution and biocompatibility of MSCs on the stroma constructs

The chemical and topographical properties of a material surface are effective and complex parameters for the adhesion ability of cells on the surface of the structures [32]. In this study, SEM analysis provided that hASCs were able to attach to the surface of the PVA-based corneal stroma constructs after 7 days of incubation. It was generally seen that nuclei were seen clearly with prominent nucleoli, and secretory granules were also seen for all constructs [41]. In Figure 10 (a, b, c), it was seen that the MSCs adhere to the surface of the constructs and spread on the entire construct. These elongated cells showed their characteristic morphology of fibroblastic tissue with a network-like structure [42-44]. In Figure 10 (c, d, e) and Figure 10 (f, g, h), it was observed fast growth and big round shapes for 13%(wt)PVA/1%(wt)CS and small round-shapes for 13%(wt)PVA/3%(wt)CS, respectively. The SEM images of the hASCs on the 13%(wt)PVA/5%(wt)CS surfaces showed a greater number of cells attached to the construct (Figure 10 (j, k, l)). Due to the outstanding biological performance, it is believed that the constructs will be ideal for corneal stromal transplantation.

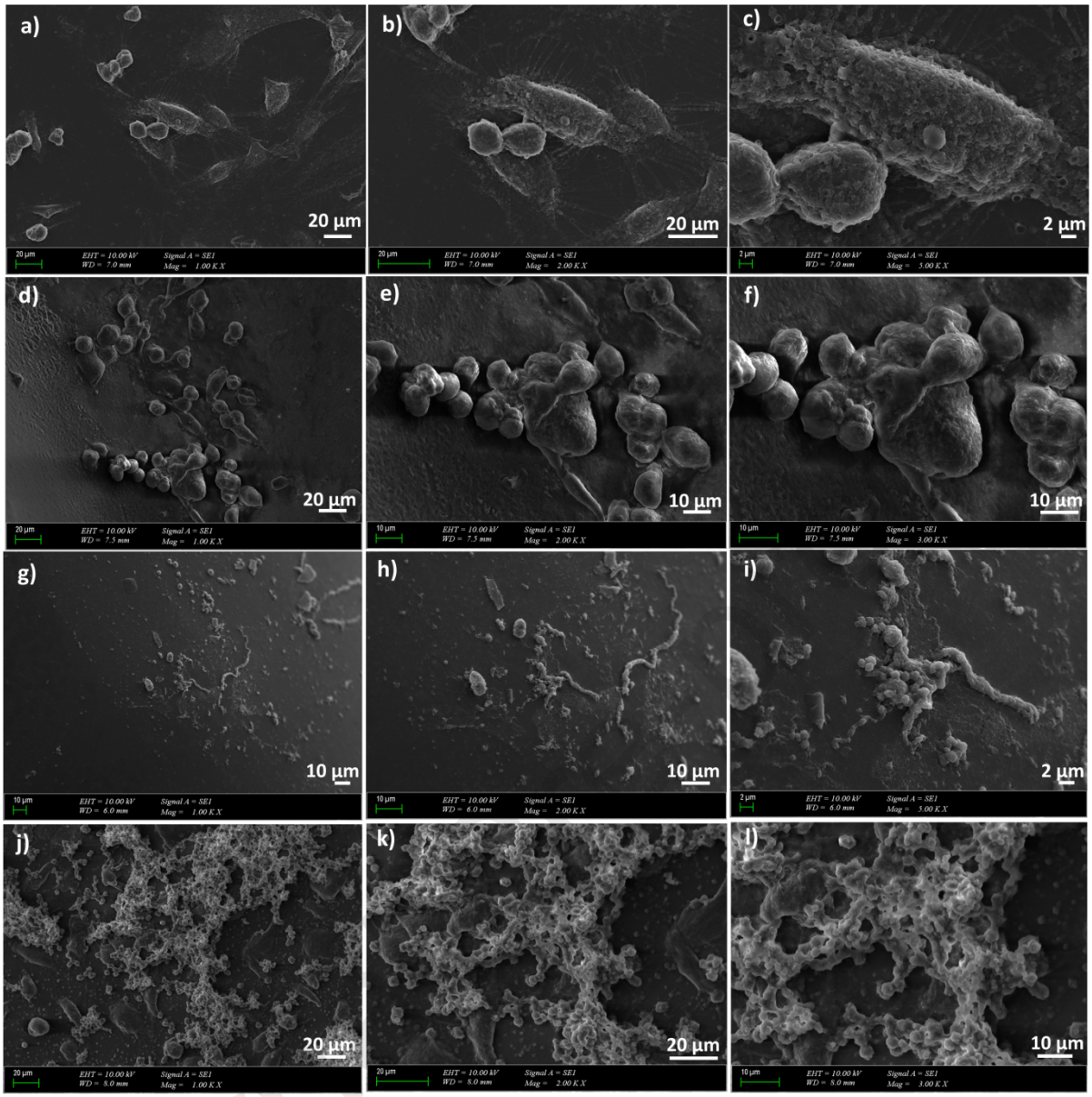

Figure 10. Cultivation of hASCs on PVA and PVA/CS blends, 13%(wt)PVA (a, b, c), 13%(wt)PVA/1%(wt)CS (d, e, f), 13%(wt)PVA/3%(wt)CS (g, h, i), 13%(wt)PVA/5%(wt)CS (j, k, l). Images were taken after 7 days of culture.

4. Conclusions

In this study, 13%(wt)PVA was blended successfully with three different amounts of Chitosan to fabricate corneal stromal constructs with efficient biocompatibility, light transmittance, and mechanical properties. Printed corneal stroma constructs were cultured with an hASC cell line to observe the viability of cells with the printed constructs. Light transmittance values showed

that CS addition decreased the transmittance percentage of 13%(wt)PVA. It is required to preserve the optical transparency of the base material when the addition of the fillers to repair the vision. SEM images demonstrated that native cornea shape was obtained successfully with appropriate dimensions and constructs displayed well-defined architecture. From this result, we concluded that 3D printing process has a tremendous potential to capture various shapes and sizes of custom cornea based on the patient population. It can be deduced from the stress-strain graph that mechanical strength values of the corneal stroma constructs are high enough to withstand intraocular pressure. The tendency of swelling was shown that CS addition increased the water absorption of the corneal stroma constructs. The degradation profile also displayed the same tendency that 13%(wt)PVA/5%(wt)CS had the maximum degradation rate compared to the others. The viability of the MSCs and cell adhesion on the surface of the constructs demonstrated that the 13%(wt)PVA/(1, 3, 5)%(wt)CS had high potential for tissue engineering structures. Even if the constructs lose their masses, the hASCs on these constructs still alive and showed also proliferation property for third and seventh days culture time. This result reported that constructs can be available for bioprinting applications for further studies.

5. Acknowledgments

The authors thank Dr. Alessandro Piombini, Dr. Orkun Ozkan, and Permtech (Italy) company for providing to determine the oxygen permeability values of the samples. The first author would also like to thank invaluable person Prof. Dr. Nilgun Baydogan for enabling the first author to use UV-spectrophotometer.

Conflict of Interest

The authors declared that there is no conflict of interest.

References

1. A. Aytimur, S. Koçyigit, I. Uslu, F. Gokmese, International Journal of Polymeric Materials and Polymeric Biomaterials. 64 (2014), 111–116.

2. H. Celebi, M. Gurbuz, S. Koparal, A. Dogan, Composite Interfaces, 20 (2013), 799-812.

3. S. M. L. Silva, C. R.C. Braga, M. V.L. Fook, C. M.O. Raposo, L. H. C. & E. L. Canedo. Application of Infrared Spectroscopy to Analysis of Chitosan/Clay Nanocomposites-Materials Science and Technology, 2012, 44-62.

4. SG. Anicuta, L. Dobre, M. Stroescu, I. Jipa, Zootehnie si Tehnologii de Industrie Alimentară, 2010, 815-822.

5. M. Ali, A. Gherissi, International Journal of Mechanical & Mechatronics Engineering IJMME-IJENS, 17 (2017), 15-28.

6. Griffith. M, Osborne. R, Munger. R, Xiong. X, Doillon. CJ, Laycock. NL, Hakim. M, Song. Y, Watsky. MA, Science, 286 (1999), 2169-2172.

7. R. Conlon, J. Teichman, S. Yeung, S. Ziai, K. Baig, JCRS Online Case Reports. 3 (2015), 29–31.

8. C. J. Rudnisky, M. W. Belin, K. Al-Arfaj, J. D. Ament, B. J. Zerbe, J. B. Ciolino, Ophthalmology. 119 (2012), 951–955.

9. L. Lin, X. Jin, Ann Eye Sci, 3 (2018), 1-8.

10. Z. Chen, J. You, X. Liu, S. Cooper, C. Hodge, G. Sutton, J. M Crook, G. G. Wallace, Biomedical materials. 13 (2018), 032002.

11. M. Kun, C. Chan, S. Ramakrishna, A. Kulkarni, K. Vadodaria, Advanced Textiles for Wound Care (Second Edition), (2019).

12. P. Yusong, D. Jie, C. Yan, S. Qianqian, Materials Technology Advanced Performance Materials, 31(2016), 5, 266-273.

13. L. Li, C. Lu, L. Wang, M. Chen, J. White, X. Hao, K. M. McLeon, H. Chen, T. C. Hughes, ACS Appl. Mater. Interfaces 10 (2018), 13283-13292.

14. A.Isaacson, S. Swioklo, C. J. Connon, Experimental Eye Research. 173 (2018), 188-193.

15. Z. Wu, B. Kong, R. Liu, W. Sun, S. Mi, Nanomaterials, 8 (2018), 124, 1-16.

16. H. C. Arca, S. Senel. Farad J. Pharm. Sci. 33 (2008), 211-226.

17. J. Chen, Q. Li, J. Xu, Y. Huang, Y. Ding, H. Deng, S. Zhao, R. Chen, Artif Organs. 29 (2005), 104-113.

18. E. A. Kamoun, X. Chen, M. S. M. Eldin, ER. S. Kenawy, Arabian Journal of Chemistry. 8 (2015), 1-14.

19. FH. Zulkifli, F. S. J. Hussain, M. S. B.A. Rasad, M. M. Yusoff, Polymer Degradation and Stability. 110 (2014), 473e481.

20. L. Zhao, H. Mitomo, M. Zhai, F. Yoshii, N. Nagasawa, T. Kume, Carbohydrate Polymers. 53 (2003), 439–446.

21. D. Z. Reinstein, T. J. Archer, M. Gobbe, R. H. Silverman, J. Coleman, J Refract Surg, 25 (2009), 776–786.

22. A. Sionkowska, A. Płanecka, J. Kozłowska, J. Skopińska-Wiśniewska, Copernican Letters, 1 (2010), 112-116.

23. M. S. Vervoort. Engineering Sciences [physics]. École Nationale Supérieure des Mines de Paris, (2006), 1-213.

24. Z. Xu, J. Li, H. Zhou, X. Jiang, C. Yang, F. Wang, Y. Pan, N. Li, X. Li, L. Shi, X. Shi, RSC Adv. 6 (2016), 43626–43633.

25. K. M. Meek, C. Knupp, Prog Retin Eye Res. 49 (2015), 1-16.

26. G. Kowalski, K. Kijowska, M. Witczak, Ł. Kuterasiński, M. Łukasiewicz, Polymers (Basel). 11 (2019), 114, 1-16.

27. M. A. Seyed, K. Vijayaraghavan, Annual Research & Review in Biology, 24 (2018), 6, 1-16.

28. S. J. Kim, S. R. Shin, Y. M. Lee, S. I. Kim, Journal of Applied Polymer Science. 87 (2003), 2011-2015.

29. A. C. Jayasuriya, K. J. Mauch, J. Biomedical Science and Engineering. 4 (2011), 383-390.

30. M. Šupová, G. S. Martynková, K. Barabaszová, Article in Science of Advanced Materials. 3 (2011), 1–25.

31. Y. Chen, X. Cao, P.R. Chang, M.A. Huneault, Carbohydrate Polymers. 73 (2008), 8-17.

32. B. Kong, S. Mi, Materials (Basel). 9 (2016), 614, 2-20.

33. T. Wang, I-J. Wang, J-N. Lu, T-H. Young, Molecular Vision. 18 (2012), 255-264.

34. B. Ozcelik, K. D. Brown, A. Blencowe, M. Daniell, G. W. Stevens, G. G. Qiao, Acta Biomaterialia. 9 (2013), 6594–6605.

35. L. Tong, SM. Saw, J. K. Siak, G. Gazzard, D. Tan, IOVS. 45 (2004), 4004-4009.

36. I. Fatt, R. S. Helen, J Optom Arch Am Acad Optom, 48 (1971), 545-55.

37. E. Altun, M.O. Aydogdu, F. Koc, M. Crabbe-Mann, F. Brako, R. Kaurmatharu, G. Ozen, S. E. Kuruca, U. Edirisinghe, O. Gunduz, M. Edirisinghe, Macromolecular Materials and Engineering, 300 (2017), 1-17.

38. S. Baghaie, M. T. Khorasani, A. Zarrabi, J. Moshtaghian, Journal of Biomaterials Science Polymer Edition. 28 (2017), 1-40.

39. J. Yi, F. Xiong, B. Li, H. Chen, Y. Yin, H. Dai, S. Li, Regen Biomater. 3 (2016), 159-66.

40. Peng L, Y. Zhou, W. Lu, W. Zhu, Y. Li, K. Chen, G. Zhang, J. Xu, Z. Deng, D. Wang, BMC Musculoskeletal Disorders 20, 257 (2019), 1-12.

41. V. A. Petrova, D. D. Chernyakov, D. N. Poshina, I. V. Gofman, D. P. Romanov, A. I. Mishanin, A. S. Golovkin, Y. A. Skorik, Materials. 12 (2019), 1-17.

42. J. Grzesiak, K. Marycz, J. Czogala, K. Wrzeszcz, J. Nicpon, Int. J. Morphol. 29 (2011), 1012-1017.

43. B. L. Banik, T. R. Riley, C. J. Platt, J. L. Brown, Front Bioeng Biotechnol. 4 (2016), 41, 1-10.

44. H. Dennaoui, E. Chouery, H. Rammal, Z. Abdel-Razzak, C. Harmouch. Stem Cell Investig. 5 (2018), 47, 1-8.

Highlights

1. 3D printing process is a promising technology to capture various shapes and sizes of custom cornea based on the patient population.
2. Mechanical properties have shown that the 3D-printed corneal stroma constructs can withstand intraocular pressure.
3. The viability of the human adipose tissue-derived mesenchymal stem cells (ADSCs) and adhesion ability of these cells on the surface of the constructs demonstrated that PVA/Chitosan blends had high potential for corneal tissue engineering structures.

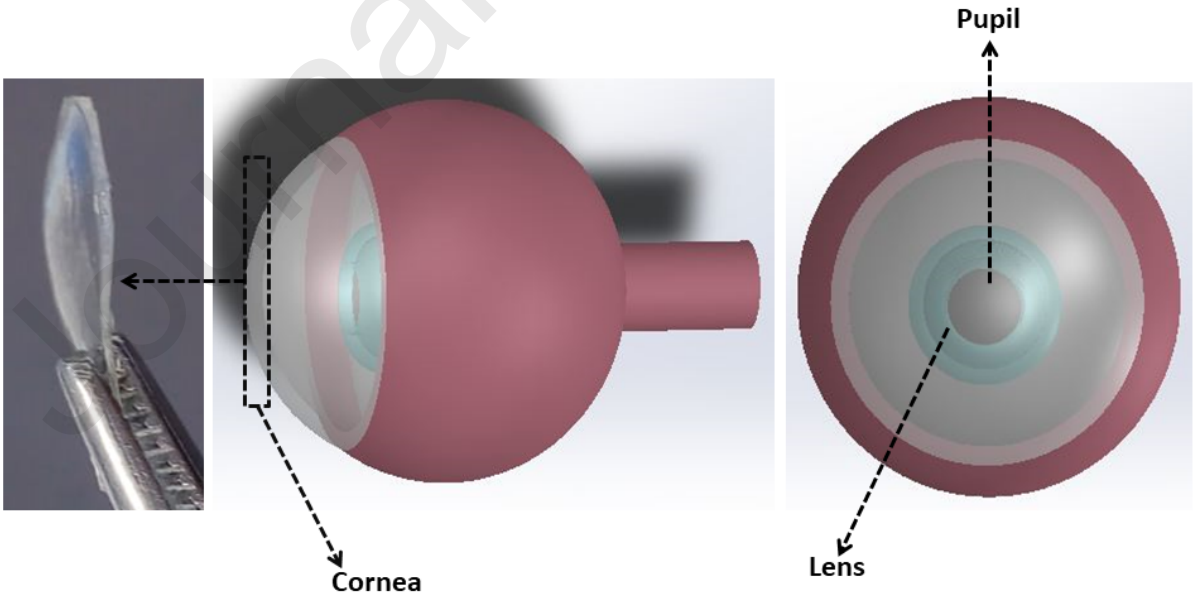

Oguzhan Gunduz: Conceptualization, Methodology **Songul Ulag and Elif Ilhan:** Methodology, Investigation, and Visualization **Ali Sahin and Betul Karademir Yilmaz:** Methodology and Investigation. **Nazmi Ekren, Osman Kilic, Deepak M. Kalaskar, Faik Nuzhet Oktar:** Investigation and Visualization.

Declaration of interests

☒ The authors declare that they have no known competing financial interests or personal relationships that could have appeared to influence the work reported in this paper.

☐The authors declare the following financial interests/personal relationships which may be considered as potential competing interests: